Quantum Dynamics in Wigner Phase Space

A Thesis

submitted to
Indian Institute of Science Education and Research Pune
in partial fulfillment of the requirements for the
BS-MS Dual Degree Programme

by

Deepesh Khushwani

Indian Institute of Science Education and Research Pune
Dr. Homi Bhabha Road,
Pashan, Pune 411008, INDIA.

May, 2023

Supervisor: Prof. T S Mahesh

Certificate

This is to certify that this dissertation entitled Quantum Dynamics in Wigner Phase Space towards the partial fulfilment of the BS-MS dual degree programme at the Indian Institute of Science Education and Research, Pune represents study/work carried out by Deepesh Khushwani at Indian Institute of Science Education and Research under the supervision of Prof. T S Mahesh, Professor, Department of Physics , during the academic year 2022-2023.

Prof. T S Mahesh

Committee:

Prof. T S Mahesh

Prof. M S Santhanam

Declaration

I hereby declare that the matter embodied in the report entitled Quantum Dynamics in Wigner Phase Space are the results of the work carried out by me at the Department of Physics, Indian Institute of Science Education and Research, Pune, under the supervision of Prof. T S Mahesh and the same has not been submitted elsewhere for any other degree.

Deepesh Khushwani

Acknowledgments

First, I would like to express my gratitude to my supervisor, Prof T. S. Mahesh, for his guidance and support over the past one and a half years. Working with him, I have learned a lot about both quantum information science and research in general.

I would like to thank my lab mates, Priya Batra, VR Krithika and Vishal Varma, for helping me in my experiments and simulations. Working in the NMR-QIP group with other group members, Arijit, Jitendra, Abhinav and Conan, has been a memorable experience. I would also like to acknowledge Sandeep Sir and Nitin Sir from the NMR lab for their constant support throughout the course of the thesis. I would also like to thank Prof. MS Santhanam and Prof. Sreejith GJ for their valuable comments and suggestions.

I also wish to thank Prof. Anisa Chorwadwala and Prof. Amit Apte for my previous projects and their availability for discussions. I would also like to thank my faculty mentor, Prof. Sudipta Sarkar, for being one of the most responsive faculty mentors and helping me with academic issues whenever needed.

Besides academics, I would also like to thank my friends at IISER for constantly supporting me throughout my thesis year and giving me memories that I will cherish all my life.

Abstract

Classical systems have a definite position and momentum, which can be visualised using a point in the phase space. Analogous treatment to classical phase space in quantum mechanics gives rise to quasi-probability distributions. One such representation is the Wigner function, which is very helpful to visualise quantum states at different points. We define and visualise the discrete Wigner function for various quantum states and their evolution. We perform experiments for the tomography of the Wigner function and find how the Wigner function can be used to find unknown quantum states. We find a computationally inexpensive method to distinguish between amplitude damping, dephasing and depolarisation channel in Wigner phase space. We also examine phase transitions from the perspective and how they connect to the Wigner phase space formalism. We also look at quantum chaos and the classical-quantum correspondence using the quantum kicked-top model.

Contents

List of Figures

List of Tables

Chapter 1

Introduction

In classical mechanics, the state of a system is described by its position and momentum. The phase space provides a way to visualize this information, thus, allowing us to understand the trajectories of the system. This also leads to a better understanding of chaos, and statistical properties of the system [1]. There have been multiple attempts for an analogous description to phase space for quantum mechanics. The reason it has been difficult to do so is that classical mechanics inherently deals with trajectories, while quantum mechanics deals with probabilities. Classical phase space has been used extensively to study phenomena in quantum mechanics, including chaos [2], dynamical tunnelling and quantum control [3]. This approach is equivalent to finding trajectories of ensembles in classical mechanics.

We, however, take a different formulation, using the quantum phase space, namely the Wigner Phase Space. This formulation is equivalent to the matrix mechanics or wave mechanics formulation, however, treating both position and momentum equally. Other quasiprobability distributions include the Husimi Q representation[4] and the Sudarshan-Glauber P-distribution[5].

The thesis starts with the theory of Wigner functions in Chapter 1. This contains Wigner's definition of the Wigner function for studying statistical mechanics [6], which was later recognized as a quantum phase space formulation by Moyal [7]. It follows with the discrete generalisation, the even-dimensional phase space [8], with discussions of the "Phase Space Point Operators", which account for a significant part of the theory of discrete generalisations of the Wigner phase space.

1.1 Wigner Functions

The Wigner function is defined as the Wigner-Weyl transform of the density matrix $\hat{\rho}$. Thus,

$$W(q,p) = \int \frac{d\lambda}{2\pi\hbar} e^{i\lambda p/\hbar} \langle q - \lambda/2|\hat{\rho}|q + \lambda/2\rangle. \tag{1.1}$$

It is the unique function which satisfies the three defining properties [9]:

1. $W(q,p)$ is real for all q and p values.

2. The overlap (Frobenius inner product) between states is given by

$$Tr[\hat{\rho}_1\hat{\rho}_2] = 2\pi\hbar \int dq\, dp\, W_1(q,p)W_2(q,p). \tag{1.2}$$

3. The integral along a line $a_1q + a_2p = a_3$ of the Wigner function gives the probability that measurement along the line, i.e., $a_1\hat{Q} + a_2\hat{P}$ has a_3 as its result. Thus, we get the following two equations:

$$\int_{-\infty}^{+\infty} dp\, W(q,p) = \langle q|\hat{\rho}|q\rangle \qquad \int_{-\infty}^{+\infty} dq\, W(q,p) = \langle p|\hat{\rho}|p\rangle. \tag{1.3}$$

   For pure states,

$$\int_{-\infty}^{+\infty} dp\, W(q,p) = |\psi(q)|^2 \qquad \int_{-\infty}^{+\infty} dq\, W(q,p) = |\phi(p)|^2, \tag{1.4}$$

   gives probability densities in q and p, respectively.

Mathematically, it can be shown that this is the only function that satisfies all three properties.

The Wigner function is a quasiprobability function. This is because the Wigner function is not a true probability function as it takes both positive and negative values. These negative values are generally provable to be small enough and do not extend beyond a few $\hbar$ values while scaling. This is due to the Heisenberg Uncertainty Principle, and thus, in the classical limit ($\hbar \approx 0$), the probability distribution is always positive. Except for the definitions of the Wigner function, we have used the units with $\hbar = 1$ in the rest of the thesis.

1.1.1 Phase Space Point operators

The Wigner function can also be written as the ensemble average of "**Phase Space point Operators**" or "**Fano Operators**" $\hat{A}$,

$$W(q,p) = Tr[\hat{A}(q,p)\hat{\rho}], \tag{1.5}$$

where the operators $\hat{A}(q,p)$ are defined as [10]

$$\hat{A}(q,p) = 1/(2\pi\hbar)^2 \int d\lambda\, d\lambda' \, \exp(-i\lambda(\hat{P}-p)/\hbar + i\lambda'(\hat{Q}-q)/\hbar). \tag{1.6}$$

These operators are very important in the discussion of the discrete generalisation of the Wigner phase space. Given the operators $\hat{A}(q,p)$, we can find the density matrix from the Wigner distribution as

$$\hat{\rho} = 2\pi\hbar \int dq\, dp\, W(q,p)\hat{A}(q,p). \tag{1.7}$$

The three defining properties of $\hat{A}(q,p)$, which lead to the three defining properties of $W(q,p)$ are:

1. $\hat{A}(q,p)$ must be Hermitian for all values of q and p.
2. $\hat{A}(q,p)$ forms a complete orthogonal set of operators. Thus,

$$Tr[\hat{A}(q,p)\hat{A}(q',p')] = \frac{1}{2\pi\hbar}\delta(q-q')\delta(p-p') \tag{1.8}$$

3. Integrating the operators along a line in phase space, we get a projection operator. Thus,

$$\int dq\, dp\, \delta(a_1 q + a_2 p - a_3)\, \hat{A}(q,p) = |a_3\rangle\langle a_3|, \tag{1.9}$$

where $|a_3\rangle$ is an eigenstate of the operator $a_1\hat{Q} - a_2\hat{P}$, with a_3 as the eigenvalue.

This Wigner function has found applications in quantum optics, information processing, electronics, quantum chemistry and signal processing [11].

1.2 Discrete Generalisation

The Wigner function forms the motivation of most definitions of finite dimensional quasiprobability distributions. The first generalisation to satisfy all required properties was given by Wootters [10] for a prime dimensional Hilbert space. Numerous others followed this, including spherical phase space, finite fields and even dimensional phase space [12], each having different properties and applicability. We focus on the even-dimensional phase space, given by Leonhardt [8].

This formulation transforms a Hilbert space of N dimensions into a Wigner phase space of $2N$ dimensions. Given the Hilbert space, we define an arbitrary basis $B_x = \{|n\rangle, n = 0, 1...N-1\}$ as the position basis. We define momentum basis states as $B_p = \{|k\rangle, k = 0, 1, ...N-1\}$, where momentum states $|k\rangle$ are given by the Fourier Transform of the position basis.

$$|k\rangle = \frac{1}{\sqrt{N}} \sum_n \exp(i\, 2\pi nk/N)|n\rangle \tag{1.10}$$

The phase space point operators $A(q,p)$ are defined using the translation operators $\hat{U}$, $\hat{V}$ and $\hat{R}$, defined as

$$\begin{aligned} \hat{U}|n\rangle &= |n+1\rangle \\ \hat{V}|k\rangle &= |k+1\rangle \\ \hat{R}|n\rangle &= |-n\rangle \end{aligned} \tag{1.11}$$

where addition is mod(N). U and V are diagonal in momentum and position basis, respectively.

$$\hat{U}^m|k\rangle = \exp(-i\, 2\pi mk)|k\rangle \qquad\qquad \hat{V}^m|n\rangle = \exp(i\, 2\pi mn)|n\rangle \tag{1.12}$$

Then, $A(q,p)$ can be given as

$$A(q,p) = \frac{1}{2N} U^q R V^{-p} \exp(i\, \pi pq/N), \tag{1.13}$$

where $q, p \in 0, 1, ...2N-1$. Then,

$$W(q,p) = Tr[A(q,p)\hat{\rho}]. \tag{1.14}$$

Although the phase space is defined in a $4N^2$ dimensional space, there are only N^2 independent Fano operators, and others can be derived from these N^2 operators by the linear relationship

$$W(q + s_q N, p + s_p N) = W(q, p)(-1)^{s_p q + s_q p + s_q s_p N} \tag{1.15}$$

for $s_p, s_q = 0, 1$. This relationship is also satisfied by the "point operators" [13]. We denote the first quadrant as G_N and full $4N^2$ dimensional space as G_{2N}. We define a line in the phase space as $L(n_1, n_2, n_3) = \{(q, p) \in G_{2N}$, such that $n_1 p + n_2 q = n_3$, with $0 \leq n_i \leq 2N-1$. Here addition is done modulo N. Two lines parameterised by the same set of integers (n_1, n_2) with different n_3 are said to be parallel. The operator $\hat{A}_L$ defined as $\hat{A}_L = \sum_{(q,p)\in L} \hat{A}(q, p)$ can be written as

$$\begin{aligned}
\hat{A}_L &= \sum_{(q,p)=0}^{2N-1} \hat{A}(q, p)\delta_{2N}\left(n_1 p - n_2 q - n_3\right) \\
&= \frac{1}{2N} \sum_{\lambda=0}^{2N-1} \sum_{(q,p)=0}^{2N-1} \hat{A}(q, p) \exp\left(-i\frac{2\pi}{2N}\lambda(n_1 p - n_2 q - n_3)\right) \\
&= \frac{1}{2N} \sum_{\lambda=0}^{2N-1} T^{\lambda}(n_1, n_2) \exp\left(i\frac{2\pi}{2N} n_3 \lambda\right),
\end{aligned} \tag{1.16}$$

where $\hat{T}(n, k)$ are called translation operators defined as

$$T(n, k) = \sum_{(q,p)=0}^{2N-1} \hat{A}(q, p) \exp\left(-i\frac{2\pi}{2N}(np - kq)\right) \tag{1.17}$$

These operators are cyclic, such that $T^N = \mathbb{I}$.

The Wigner function satisfies the following properties in analogy with the continuous Wigner function:

1. As the operators $\hat{A}(q, p)$ are Hermitian, $W(q, p)$ is real for all values of q and p.

2. The Frobenius inner product of two states is given as

$$Tr[\rho_1 \rho_2] = N \sum_{\alpha \in G_{2N}} W_1(\alpha) W_2(\alpha). \tag{1.18}$$

3. As $T^N = \mathbf{I}$, the eigenvalues of the operator T should be the eigenvalues of unity, with the form $\exp(-i2\pi\phi_j/N)$ with eigenvectors $|\phi_j\rangle$, where ϕ_j are integers. Thus,

$$\hat{A}_L = \sum_{j=0}^{N} \delta_{2N}(2\phi_j - n_3)|\phi_j\rangle\langle\phi_j|. \tag{1.19}$$

Therefore, $\hat{A}_L$ are projection operators onto a subspace generated by a subset of the eigenvectors of the translation operator $\hat{T}(n_1, n_2)$. The dimensionality d of this subspace is given by the trace of $\hat{A}_L$. In qubit systems, N is always even whether we work with density matrices or their partial traces. Hence, d is given as

$$d = 1/2 \sum_{\lambda=0}^{N-1} \delta_N(\lambda n_1)\delta_N(\lambda n_2) \exp\left(i\frac{2\pi}{2N}m\lambda\right)[1 + (-1)^{n_3}] \tag{1.20}$$

Thus, for odd n_3, the sum over a line is always 0. For a line, L_q defined as $q = n_3$, the Wigner function summed over it is given by

$$\sum_{(q,p)\in L_q} W(q,p) = \sum_{p} W(n_3,p) = \langle n = n_3/2|\hat{\rho}|n = n_3/2\rangle \tag{1.21}$$

for even n_3 and 0 for odd n_3. The same follows for the line L_p defined as $p = n_3$. This is the discrete equivalent of the property 1.3.

$\hat{A}(\alpha)$ form a complete set in G_N with the following identity.

$$Tr[\hat{A}(\alpha)\hat{A}(\alpha')] = \delta_N(q - q')\delta_N(p - p') \tag{1.22}$$

with $\delta_N(x) = 1/N \sum_{n=0}^{N-1} e^{2\pi i x}$. $\delta_N(x)$ is the "periodic delta function", which is zero unless $x = 0\, mod$ N. Given these operators, we can write the density matrix as a one-to-one function of the Wigner phase space as

$$\begin{aligned} \hat{\rho} &= N \sum_{\alpha\in G_{2N}} W(\alpha)A(\alpha) \\ &= 4N \sum_{\alpha\in G_N} W(\alpha)A(\alpha) \end{aligned} \tag{1.23}$$

for all the valid Wigner phase space representations. Given a unitary process $U(t)$ acting on

the density matrix ρ such that

$$\rho(t) = U(t)\rho(0)U(t)^{\dagger}, \tag{1.24}$$

the evolution in phase space is given by the matrix $Z_{\alpha\beta}$. Thus,

$$W(\alpha, t) = \sum_{\beta \in G_{2N}} W(\beta, 0) Z_{\alpha\beta} \tag{1.25}$$

$$Z_{\alpha\beta} = NTr[\hat{A}(\alpha) U \hat{A}(\beta) U^{\dagger}] \tag{1.26}$$

In this thesis, we have studied phenomena such as Quantum chaos, characterization of noise processes and Quantum Phase Transitions using the Discrete Wigner Formalism. We have also performed experimental characterisation of quantum chaos using the Wigner functions in NMR architecture. Chapter 2 contains experimental details of the project, including quantum circuits, details of molecules and a short introduction to Nuclear Magnetic Resonance (NMR) Quantum Information Processing (QIP). Chapter 3 provides the results of the numerical simulations and experiments, with details about quantum phenomena explored using the Wigner phase space, including phase transitions and quantum kicked top. Chapter 4 contains the conclusions based on the methods and the results.

Chapter 2

NMR Experiments

2.1 Theory

NMR is a spectroscopic technique based on the nuclear spins of certain isotopes. The spin leads to a magnetic moment, which precesses in the presence of a strong magnetic field [14]. For atoms with nonzero nuclear magnetic spin quantum number I, this leads to a splitting in energy levels, called the Zeeman effect. These energy levels are given by

$$E_m = \gamma m B_0, \tag{2.1}$$

where B_0 is the applied magnetic field, γ is the gyromagnetic ratio of the atom, and m is the magnetic quantum number, which takes $2I+1$ values from $\{-I, -I+1 ... I-1, I\}$. The corresponding frequency of transitions is the Larmor Frequency

$$\omega_0 = -\gamma B_0 \tag{2.2}$$

Absorption of frequency is called resonant when spins with a given ω_0 are perturbed by an external magnetic field of the same frequency. This phenomenon is called Nuclear Magnetic Resonance[15]. NMR happens in nuclei with a nonzero I, called NMR active nuclei. For quantum information processing purposes, we generally use nuclei corresponding to $I = 1/2$.

The internal Hamiltonian of a system with one spin-1/2 atom is given by

$$H_0 = \omega_0 I_z, \tag{2.3}$$

where $I_z = \sigma_z/2$, thus, it behaves as a two-level system–a qubit. Qubits are quantum analogues of the two-level systems called bits, used in classical computation.

2.1.1 Qubit states

For n coupled spin-1/2 nuclei, the internal Hamiltonian is given as [16]

$$H_0 = \sum_{i=1}^{n} \omega^i I_z^i + 2\pi \sum_{i<j}^{n} J_{ij} I^i \cdot I^j. \tag{2.4}$$

Here n is the number of qubits, J_{ij} is the scalar coupling, and ω_i is the Larmor frequency. Under the weak coupling approximation i.e., $|J_{ij}| \ll |\omega_i - \omega_j|$, we can drop the xx and yy terms and simplify to the secular Hamiltonian form

$$H_0 = \sum_{i=1}^{n} \omega^i I_z^i + 2\pi \sum_{i<j}^{n} J_{ij} I_z^i I_z^j. \tag{2.5}$$

NMR qubits are initialized in the thermal equilibrium state at temperature T, following Boltzmann distribution. This state is given as

$$\rho_{eq} = \frac{e^{-H_0/k_B T}}{Tr[e^{-H_0/k_B T}]}. \tag{2.6}$$

where H_0 is the internal Hamiltonian. At room temperature, the energies $E_i \ll k_B T$. Thus, using Taylor expansion for n qubits,

$$\begin{aligned} \rho_{eq} &\approx \mathbf{I}/2^n - \frac{H_0}{2^n k_B T} \\ &\approx \mathbf{I}/2^n + \sum_{i=0}^{2^n-1} \frac{\omega_{0i}}{2^n k_B T} I_z^i. \end{aligned} \tag{2.7}$$

The first part is the identity matrix which plays no role in the signal. The second part is called the **traceless deviation matrix** ρ_I, which contributes to the signal. This part is inversely

proportional to 2^n and, thus, severely limits the scalability of NMR quantum simulators. This part is very small compared to the total density matrix, making NMR states highly mixed. However, it is possible to prepare **pseudo-pure states (PPS)**, which can effectively mimic the dynamics of pure states [17]. These states have a deviation matrix proportional to the effective traceless representation of the pure state. Similarly, an entangled NMR state obtained at room temperature is always pseudo-entangled.

2.1.2 Quantum gates

NMR nuclei typically have radio frequency (rf) range energy differences. Thus, single qubit gates can be experimentally realized using rf frequency pulses, defined by their amplitude, phase and duration. For a single-qubit system, given an rf pulse, we have the Hamiltonian

$$\begin{aligned} H^{tot}(t) &= H_0 + H^{rf}(t) \\ &= \omega_0 I_z + \omega_1 [I_x \cos(\omega_{rf} t + \phi) + I_y \sin(\omega_{rf} t + \phi)]. \end{aligned} \tag{2.8}$$

Here, $\omega_1 = -\gamma B_1$ is the rf amplitude, with B_1 as the applied magnetic field. We convert it to a time-independent effective Hamiltonian using the interaction picture. Thus,

$$H_e = \Omega I_z + \omega_1 [I_x \cos(\phi) + I_y \sin(\phi)]. \tag{2.9}$$

Here $\Omega = \omega_0 - \omega_{rf}$ is the offset frequency. An initial state $\rho(0)$ evolves under this Hamiltonian in time τ as

$$\rho(\tau) = e^{-iH_e\tau} \rho(0) e^{iH_e\tau}. \tag{2.10}$$

Similarly, these gates can be applied to multiple qubits. However, they also evolve under the coupling Hamiltonian $2\pi J I_z S_z$, where I_z and S_z are z spin matrices of the two qubits. For a given J, any effective rotation angle can be realized by changing the pulse time.

Generally, we use short-duration hard pulses, which have wide bandwidth in the frequency spectrum. Such pulses uniformly affect multiple resonance frequencies. However, in some cases, for example, specific spin selection in homonuclear systems or in case of significant rf inhomogeneity, we use short pulses with low bandwidth in the frequency domain (soft pulses) and other specific methods to create selective pulses, called optimal control algorithms, for example, GRAPE [18].

2.2 Experimental Details

All the experiments were liquid-state NMR experiments on a Bruker 500 MHz NMR spectrometer at an ambient temperature of 300 K and on resonant conditions.

2.2.1 Quantum Circuit for Wigner space tomography

As $W(q,p)$ is the expectation value of the operator $A(q,p)$, it can be directly measured for a given state using the circuit in Figure 2.1 [19].

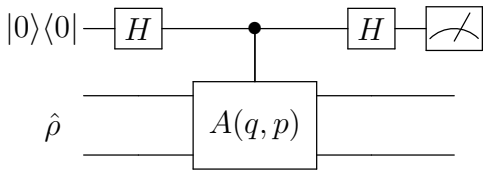

Figure 2.1: Quantum Circuit for direct measurement of $W(q,p)$

We use this, and the decomposition $A(q,p)$ as 1.13 to get the whole circuit as consisting of four total operators applied multiple times- cR, cV^{-1}, cU and $R_z^1(\pi/4)$, where cO is operator O operating on the last two qubits with control on the first. $R_z^1(\pi/4)$ is an operator that rotates the first spin along the z-axis by an angle of $\pi/4$, given by $\exp(-iI_z\pi/4)$.

This circuit has been optimized in the experiments using GRAPE and Push-Pull [20] optimization techniques to find optimal pulses for the circuit. We perform experiments for two qubits with one qubit as the ancilla, i.e., using $2+1$ qubit systems. We only find the first N^2 entries in the Wigner phase space, using the measurement circuit with appropriate re-scaling and the other $3N^2$ using the linear relationship (1.15).

2.2.2 Experimental samples

We experimentally study the discrete phase space distribution for two qubits using two samples of three qubits each, as explained below.

DBFM

We used ^{19}F and ^{13}C nuclei as the system and the ^{1}H nucleus as the ancillary qubits of the molecule Dibromofluoromethane (DBFM) with labelled carbon (C-13) dissolved in acetone-D6. The phase space points were determined using hard pulses, while GRAPE was used to prepare PPS [21]. The simplified circuit is given in the figure 2.2.

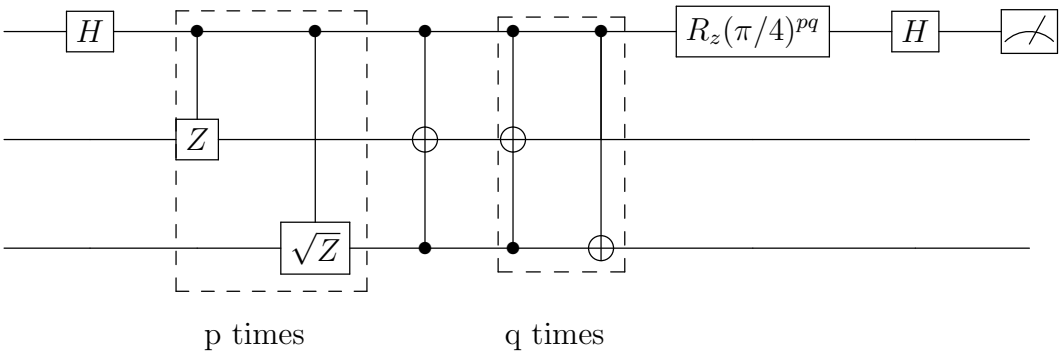

Figure 2.2: Simplified Circuit for direct measurement of $W(q,p)$, used for DBFM

The couplings of the molecule are given in the table 2.1.

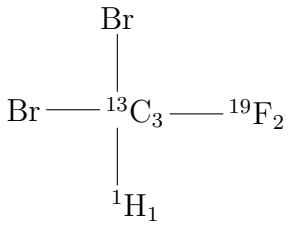

Figure 2.3: Molecular Structure of the DBFM molecule

^{1}H (Hz)	^{19}F (Hz)	^{13}C(Hz)		T_2(s)	T_1(s)
0	49.7	224.5	^{1}H	0.3	13.7
	0	-310.9	^{19}F	0.2	5.2
		0	^{13}C	0.5	1.9

Table 2.1: Chemical Shifts (diagonal elements) and J-coupling constants for the DBFM molecule, with relaxation times T_1 and T_2

During these experiments, we found a source of error being nonlinearity in the carbon channel of the spectrometer, which resulted in calibration errors in the GRAPE pulses. This led us to change our sample in the experiments, for which we selected the molecule Trifluoroiodoethene (TFIE).

TFIE

As the experiment for nonlinear effects was not very successful in DBFM due to nonlinearities in the C-13 channel of the spectrometer, we continued that experiment with another molecule containing no labelled carbon. We used TFIE dissolved in acetone-D6 as it has good coupling and high chemical shifts, thus, making it easier to address each spin separately. The coupling constants for the Hamiltonian are given in the table 2.2.

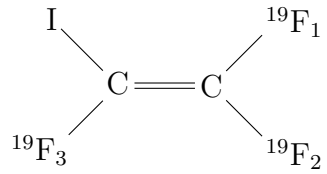

Figure 2.4: Molecular structure of the TFIE molecule

$^{19}F_1$ (Hz)	$^{19}F_2$ (Hz)	$^{19}F_3$(Hz)		T_2^*(s)	T_1(s)
11841	69.9	47.7	$^{19}F_1$	0.8	6.9
	0	-128.2	$^{19}F_2$	0.8	7.5
		-17293	$^{19}F_3$	0.6	6.2

Table 2.2: Chemical Shifts (diagonal elements) and J-coupling constants for the TFIE molecule, with relaxation times T_1 and effective relaxation time T_2^*

We prepared the PPS using the circuit given in [22]. However, instead of the Gaussian selective pulses, we use GRAPE to create pulses as gaussian pulses are generally more prone to rf inhomogeneity, which can affect our experiment.

As the circuit has a large number of gates for a given (q, p), we use a different pulse for performing the gate $c(U^q R)$ for the four values of q. Because of this, the total pulse duration can be shortened, and thus, our pulses are less prone to rf inhomogeneity. Other

than that, the gates simplify quite a bit, and given that our cV^{-1} pulse works well under rf inhomogeneity, we need to create four pulse sequences instead of two.

Chapter 3

Results

In this chapter, we will discuss the results of the numerical simulations and experiments. We will start with results about state tomography, noise, and phase transitions and finally look at results in nonlinearity based on the quantum kicked top.

3.1 Wigner Phase Space Tomography

As a result of 1.15 and 1.3, we find the normalisation condition for the even-dimensional Hilbert space:

$$\sum_{(q,q)\in G_N} W(2q, 2p) = 1, \tag{3.1}$$

$$\implies \sum_{(q,p)\in G_{N/2}} W(2q, 2p) = \frac{1}{4}. \tag{3.2}$$

This is only for even values in G_{2N} because given 1.15, all the odd values of (q, p) have a negative of them in the phase space. This condition then corresponds to the condition that $Tr[\rho] = 1$, thus, making all probabilities sum to one. We also note only the even rows/columns give probabilities when summed up. For a given even row with $p = p_0$ in the

quadrant G_N, we have the positivity conditions:

$$|\sum_{odd\ q} W(q,p_0)| \leq \sum_{even\ q} W(q,p_0). \tag{3.3}$$

Similarly, for even column with $q = q_0$, in the quadrant G_N,

$$|\sum_{odd\ p} W(q_0,p)| \leq \sum_{even\ p} W(q_0,p). \tag{3.4}$$

This condition ensures that the probabilities p$(q_0/2)$ and p$(p_0/2)$ are always positive.

Similarly, for a state to be pure, purity should be equal to one. Thus, using 1.18

$$\begin{aligned} & Tr[\rho^2] = 1 \\ \implies & N \sum_{\alpha \in G_{2N}} W(\alpha)^2 = 1 \qquad (3.5) \\ \implies & 4N \sum_{\alpha \in G_N} W(\alpha)^2 = 1. \qquad (3.6) \end{aligned}$$

3.1.1 Position and momentum eigenstates

For a position eigenstate(computational basis), we get $\rho_{q_0} = |q_0\rangle\langle q_0|$. We can easily solve the equation for the Wigner function of this state as [13]

$$\begin{aligned} W(q,p) &= \frac{1}{2N}\langle q_0|U^q R V^{-p}|q_0\rangle \qquad (3.7) \\ &= \frac{1}{2N}\delta_N(q-2q_0)(-1)^{p(q-2q_0)_N}. \qquad (3.8) \end{aligned}$$

Here $z_N = z(mod\ N)$. This corresponds to two vertical strips, a constant positive strip $W = 1/2N$ at $q = 2q_0$ and an oscillating strip at $q = 2q_0 \pm N$, with $W = 1/2N$ for even values of p and $W = -1/2N$ for odd values of p. A similar behaviour is seen for momentum eigenstates, with the strips being horizontal instead of vertical.

For a linear superposition state, $|\psi\rangle = (|q_0\rangle + e^{i\phi}|q_1\rangle)/\sqrt{2}$, we get four strips corresponding to two each of q_0 and q_1, and two fringes showing the interference between the two states at $(q_0 \pm q_1)_N$.

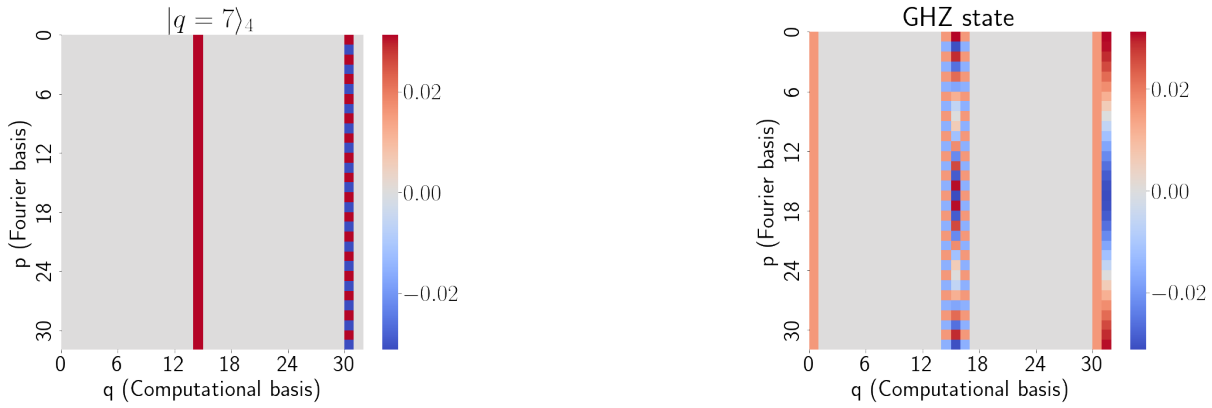

(a) Position Eigenstate
$|\psi\rangle = |0111\rangle$

(b) GHZ state
$|\psi\rangle = (|0000\rangle + |1111\rangle)/\sqrt{2}$

Figure 3.1: Wigner function of two simple states

The equation 1.21 implies that the even numbered rows and columns of the Wigner Phase Space signify the probabilities, and the odd numbered signify the coherence or interference in the given basis. Thus, given a position basis, the diagonal terms of the density matrix are denoted by the even columns, and the non-diagonal terms by the odd columns of the Wigner distribution. Hence, we see that a position eigenstate has two vertical strips at even numbered points, but is totally delocalised in the momentum space, and vice versa which also comes from the Heisenberg Uncertainty Principle.

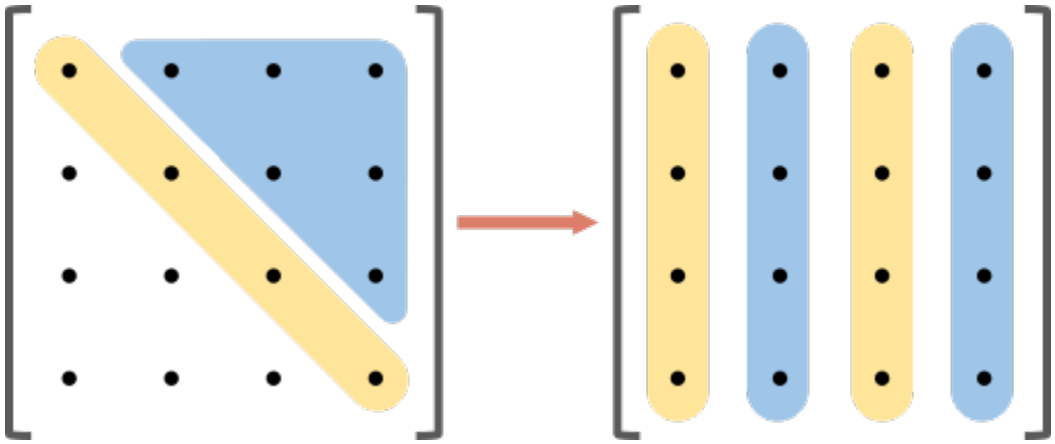

Figure 3.2: When the density matrix elements are transformed to the Wigner Phase Space, the even numbered columns (starting from 0) are related to the populations (diagonal elements) in the computational basis and the odd numbered columns are related to the coherences (off-diagonal elements).

Thus, a state that is localised in the Wigner Phase Space is the state which has the least uncertainty product in the position and momentum. In the continuous Wigner function formalism, that state is the Gaussian wave packet. We found that Gaussian states, i.e., states with populations that follow a Gaussian distribution are highly localised in the Wigner Phase Space for a large Hilbert Space just like the continuous case (Fig 3.3). We explore such states in more detail in the section 3.4.

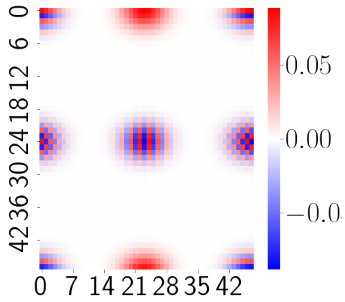

Figure 3.3: A spin 11.5 (24 dimensional Hilbert Space) Gaussian state

For the experiments, we use Frobenius inner product as the fidelity, defined for two states ρ_1 and ρ_2 as

$$F(\rho_1, \rho_2) = Tr[\rho_1 \rho_2]. \tag{3.9}$$

As the Frobenius norm, given by $Tr[\rho^2]$ of mixed quantum states is less than one, the fidelity of mixed quantum states with themselves is less than one. Thus, this measure of fidelity only works if our expectation of the final state is a pure state. As all our experiments are theoretically supposed to give pure state results, we argue that using Frobenius inner product as a measure of fidelity makes sense.

3.1.2 Experimental Results

We used the Wigner Phase Space Tomography to visualise basic quantum states experimentally. The fidelities are calculated using the relation 1.18. For a given value of α, we call $W(\alpha)$ as a pixel. We perform the whole run of the quantum circuit to calculate one pixel of the Wigner Phase Space.

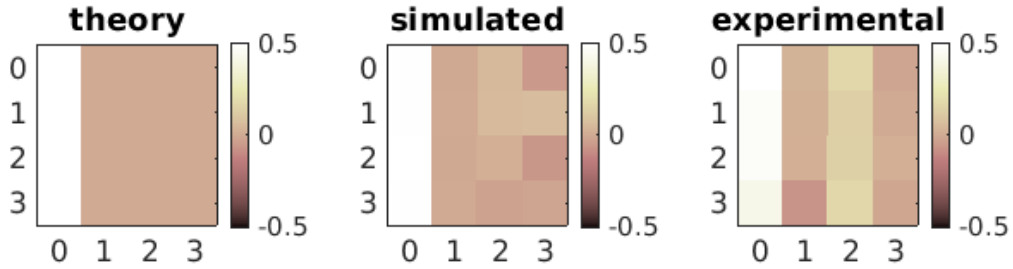

(a) 2 qubit $|00\rangle$ state with experiment to theory fidelity 0.9426

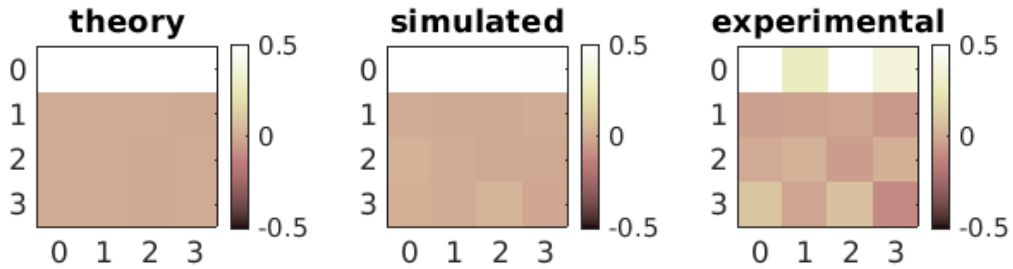

(b) 2 qubit $|++\rangle$ state with experiment to theory fidelity 0.9387

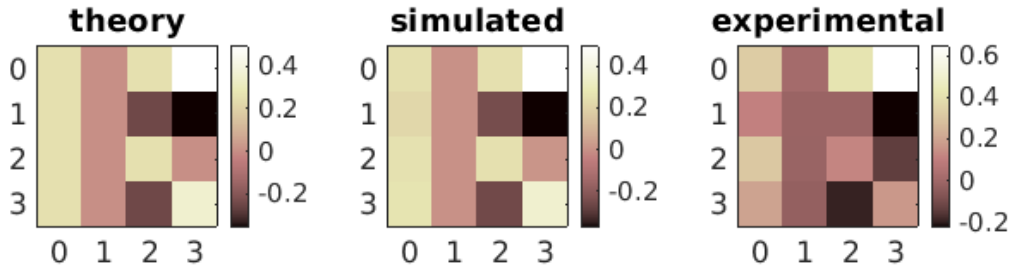

(c) Bell state, $(|00\rangle + |11\rangle)/\sqrt{2}$ with experiment to theory fidelity 0.8837

Figure 3.4: Wigner function of a few eigenstates. The first column shows the theoretical prediction. The second column shows the simulation with the GRAPE pulses, and the third column shows the experimental result.

We see that our tomography circuit works fairly well for product states, with fidelities around 0.94. However, the experiments have a larger error in case of entangled states, with fidelities around 0.88. This can happen because of errors in both state preparation, as well as tomography of the states.

One limitation in our approach to measure Wigner Phase Space directly is that the resulting Wigner Phase Space, even on small errors can be non-physical (i.e., can correspond to invalid density matrices). In our case, that happened for an error of 5% in calculating the individual pixels of the Wigner Phase Space. For such cases, tricks used for quantum state tomography can be useful. For example, having an equality constraint like 3.1 can help us get normalized Wigner function, and can also reduce the number of experiments by one. However, even taking that into consideration, we found that sometimes, the conditions 3.3 and 3.4 are not satisfied.

3.2 Noise Characterization

Given operator U acting on a state ρ, we have a simple vector transformation $Z_{\alpha\beta}$ between original Wigner Phase Space $W(\alpha)$ and final phase space $W(\beta)$, where $\alpha = (q_\alpha, p_\alpha)$. In the Liouville space, noise processes can be modelled using the operator sum representation of Kraus operators [23],

$$\rho(t) = \sum_m K_m(t)\rho(0)K_m^\dagger(t). \tag{3.10}$$

For such a process, we prove that the final matrices $Z_{\alpha\beta}$ can be written as the sum of all the individual operators, i.e.,

$$Z_{\alpha\beta}^f = \sum_m Z_{\alpha\beta}^m. \tag{3.11}$$

We numerically simulated the Wigner function for three noise channels, which are essential in experimental studies - depolarization, dephasing and amplitude damping channels [23], for global noise channels in two qubit systems. We studied the three channels both qualitatively and quantitatively to understand how noise manifests itself in the Wigner Phase Space. We found the following qualitative changes -

1. The contrast between the colours of the Phase Space decreased for increasing intensity of noise. This was constantly seen for dephasing and depolarization, but for amplitude damping, extra contrast is seen in the phase space.

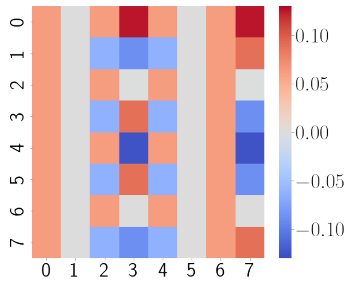

(a) $|\Phi^+\rangle$

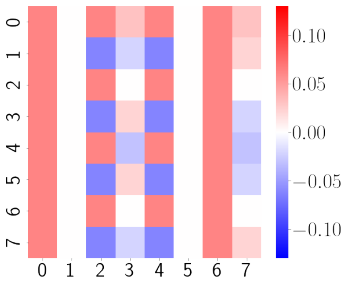

(b) 50% dephasing

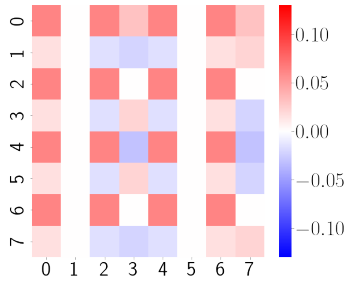

(c) 50% depolarization

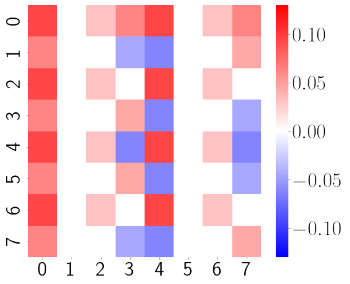

(d) 50% amplitude damping

Figure 3.5: state $|\Phi^+\rangle$ under different noise channels

2. The number of non-zero values first increased, then they started to decrease as the state changed to a mixed state. We studied this property using the entropy of the Wigner Phase Space distribution. We did this by binning it to a probability distribution and calculating the Shannon entropy of the function.

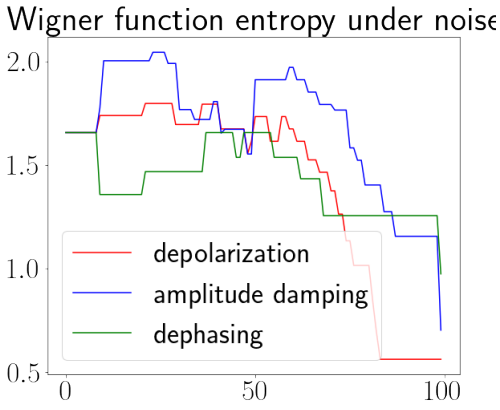

Figure 3.6: $|\Phi^+\rangle$ under noise. The x-axis is the noise strength, the y-axis is the entropy.

3. For states with an equal contribution of 0s and 1s in their representations, the depolarization and dephasing channels have similar dynamics, which is what we expect.

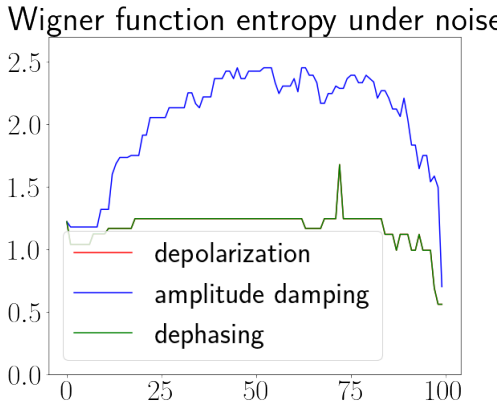

Figure 3.7: $|{+}{+}\rangle$ under noise. The x-axis is the noise strength, and the y-axis is the entropy.

To characterize noise dynamics using the equation 3.11, we found the matrix $Z^f_{\alpha\beta}$ for the three channels on 2 qubits in a global noise scenario, i.e., same form of noise acting on both the qubits. Another assumption is that the noise acts independently on all the qubits. We found that the total Z^{tot} is given as

$$Z^{tot} = a\mathbf{I} + bZ^{amp} + cZ^{deph} + dZ^{depol}, \tag{3.12}$$

where Z^{amp}, Z^{deph}, and Z^{depol} are the matrices $Z^f_{\alpha\beta}$ for the amplitude damping, dephasing and depolarization channel for full noise strength. This acts on the Wigner function as

$$W_{noise} = Z^{tot} W_{predicted}. \tag{3.13}$$

We find the Wigner functions with individual contributions of the different forms of Z, to find that

$$W_{noise} = aW_{predicted} + bW_{amp} + cW_{deph} + dW_{depol}. \tag{3.14}$$

For only one channel acting on the qubits, we found that a least squares regression on W_{noise} gives the coefficient of the channel and its compliment for a. For example, for an amplitude damping channel of strength 0.6 acting on the qubits, we get $b = 0.6, a = 0.4$, and the other two coefficients as 0. For multiple channels acting on the qubits but in an independent global noise process, we find that least squares regression gives all four coefficients.

3.3 Phase transitions

We numerically study phase transitions at zero temperature (ground state phase transition) in two Ising-type models in the Wigner phase space. First, we studied the transverse Ising model [24]. To start with, we assumed all-to-all interaction, thus, giving the Hamiltonian

$$H(a, J) = a \sum_i \sigma_x^i + J \sum_{i<j} \sigma_z^i \sigma_z^j. \tag{3.15}$$

Here, a is the transverse field strength, J is the Ising coupling strength and $|J| \gg a$. Here, σ_x^i, σ_z^i are the Pauli spin matrices at site i. When $J > 0$, the system is a frustrated spin system, and the interactions of the Ising model are of the antiferromagnetic type. However, when $J < 0$, the system is non-frustrated and the interactions are ferromagnetic.
We simulated the Wigner phase space for multiple values of the parameter J/a to find signatures of phase transitions in the Wigner phase space model. We found the following -

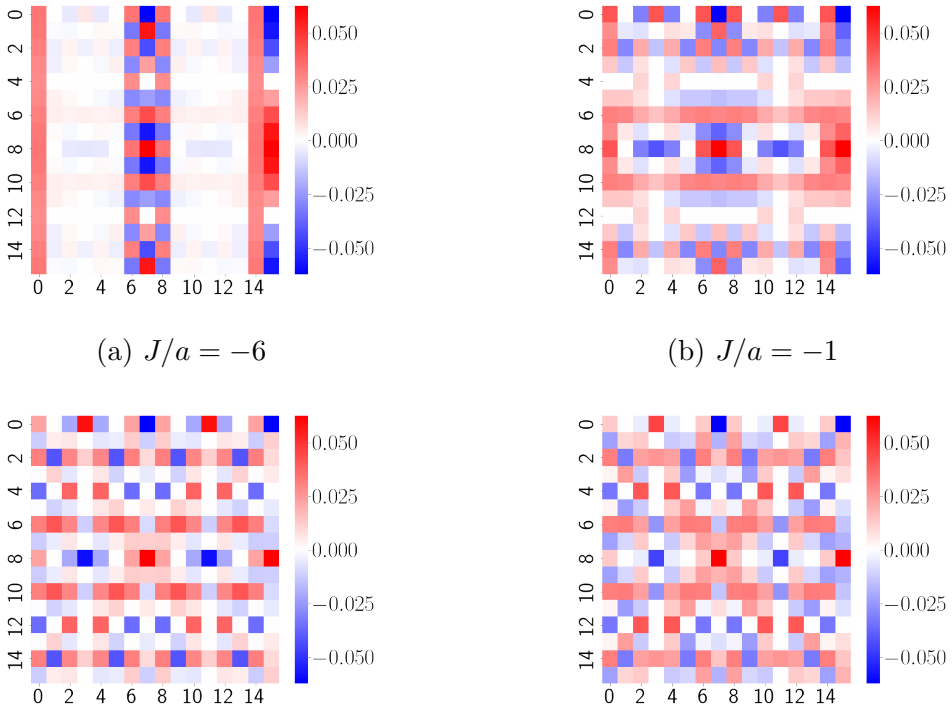

(a) $J/a = -6$ (b) $J/a = -1$

(c) $J/a = 0.7$ (d) $J/a = 6$

Figure 3.8: Ground state of the system for different values of the parameter J/a

1. The Wigner function changed its qualitative nature from the negative to positive values of the parameter J/a (Figure 3.8).

2. Approaching the phase transition, $J/a = 0$, the Wigner function simplifies as a whole in a continuous way.

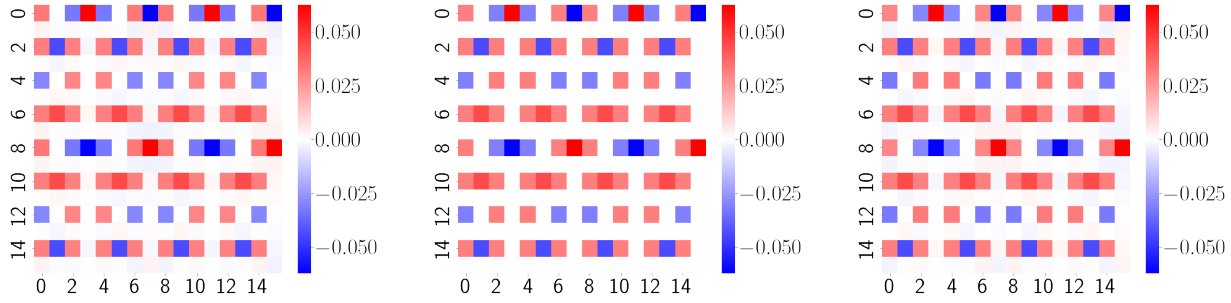

(a) $J/a = -0.1$ (b) $J/a = 0$ (c) $J/a = 0.1$

Figure 3.9: Wigner function near $J/a = 0$

3. To quantify this, we plotted the entropy of the Wigner function, which has a sharp dip at the point of phase transition, which becomes sharper with the number of bins. We have plotted the same for entropy calculated according to 80 bins.

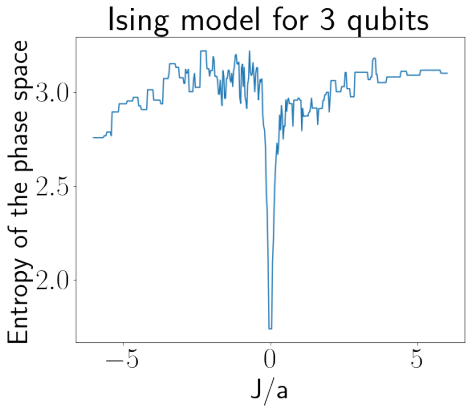

Figure 3.10: Entropy for the 3 qubit Ising model

For a 4-qubit model, we get the following figure while calculating the entropy. We take the 4 qubits in a linear chain instead of an all-to-all coupling as it is very tough to find such a system in nature.

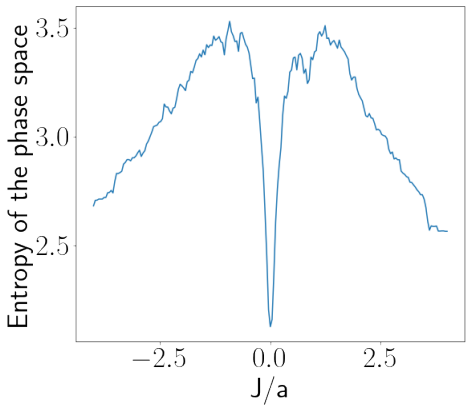

Figure 3.11: Entropy for the 4 qubit Ising model

After finding a strong signature of phase transitions in this model in the Wigner Phase Space, we studied another model of phase transitions, defined by the Hamiltonian

$$H(B_z) = \sigma_z^1 \sigma_z^2 + B_z(\sigma_z^1 + \sigma_z^2). \tag{3.16}$$

This Hamiltonian has the eigenvalues $1 + 2B_z, -1$ and $1 - 2B_z$ for the states $|00\rangle, |\phi^+\rangle$ and $|11\rangle$. The symmetry of the Hamiltonian does not allow evolution to the singlet state [25]. These energy values lead to a phase transition at $B_z = 1$ and $B_z = -1$. We see in the figure 3.12, that there is a discontinuity at the points of phase transition. This time, however, the discontinuity is not a sharp dip.

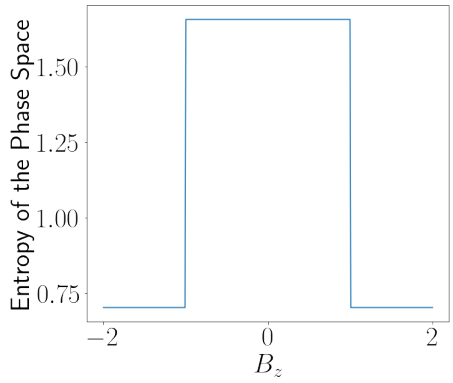

Figure 3.12: Wigner Space Entropy of the ground state

However, we find that the phase transition in this model is not experimentally possible due to the level crossings at the points of phase transitions [26]. To study experimental dynamics, we add a small term $B_x(\sigma_x^1 + \sigma_x^2)$ to the Hamiltonian. As the value of this term increases, the phase transition becomes less visible as the difference in energy due to the B_x term will take over the phase transition due to the energy difference of the other two terms.

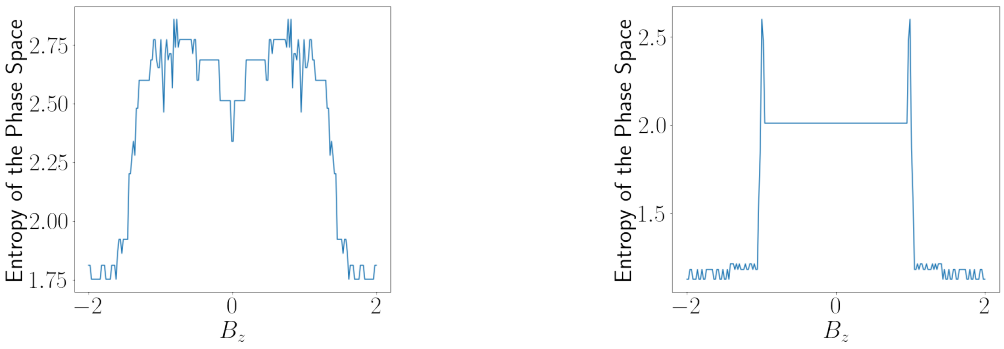

(a) $B_x = 0.1$ (b) $B_x = 0.001$

Figure 3.13: Entropy of the Wigner function for two different values of B_x

However, trying to perform adiabatic evolution of the Hamiltonian, we find that the phase transitions are seen clearly even at B_x values as high as 0.1. This effect implies that using this method will help understand phase transitions even in scenarios when the normal experimental procedures lead to a problem as level crossings and infinite time can not be achieved in real experimental systems.

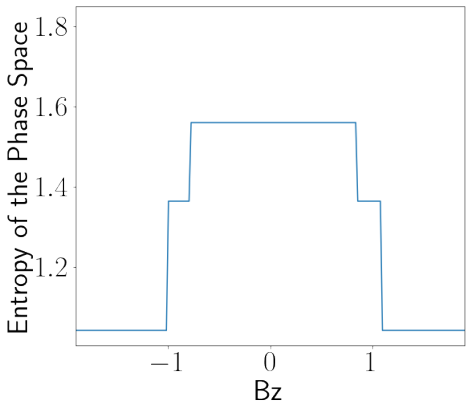

Figure 3.14: Entropy of the adiabatically evolved model when $B_x = 0.1$

While measuring phase transitions using the Wigner Phase Space, we find that sometimes, there is a dip in the entropy, and sometimes, there is just a discontinuity, or a very large jump. Thus, the measure itself keeps changing. This also signifies the problem of studying phase transitions, which has been puzzling people for a long time. Also, our method gives discontinuities at points which are not proven to be points of phase transitions. It could be due to either using large number bins for calculation of entropy, which is necessary to detect phase transitions or just an artefact of the specific phase space distribution function.

3.4 Nonlinear Quantum Dynamics

To explore nonlinearity in the phase space dynamics, we used the "Quantum Kicked Top" model. We looked at the dynamics of the Wigner phase space under the Kicked Top Hamiltonian, and looked at multiple measures as the signatures of chaos.

3.4.1 Quantum Kicked Top

The Quantum Kicked Top is given by the Hamiltonian [2],

$$H = \frac{k}{2j\tau} J_z^2 + pJ_x \sum_{n=-\infty}^{n=+\infty} \delta(t - n\tau), \tag{3.17}$$

where J_x, J_y and J_z are the x, y, z components of the angular momentum operator $\mathbf{J}$. τ is the time period, and k is the chaoticity parameter. This model shows periodic trajectories for $k < 1$ and chaotic trajectories for large k. The intermediate chaoticity values lead to a mixed behaviour, with both chaotic and periodic trajectories depending on the initial conditions. We study the classical trajectories in polar coordinates (θ, ϕ), with $p = \pi/2$.

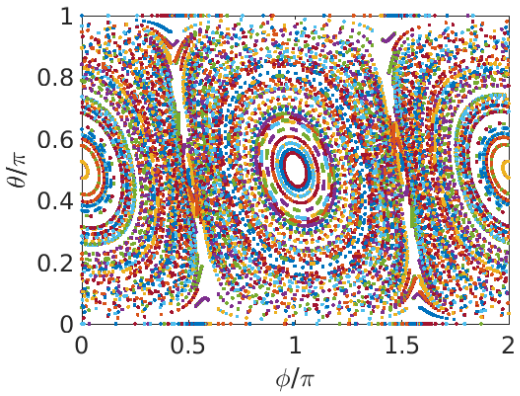

(a) $k = 0.5$

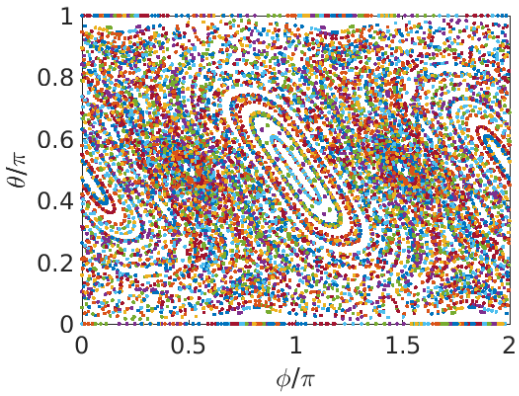

(b) $k = 2.0$

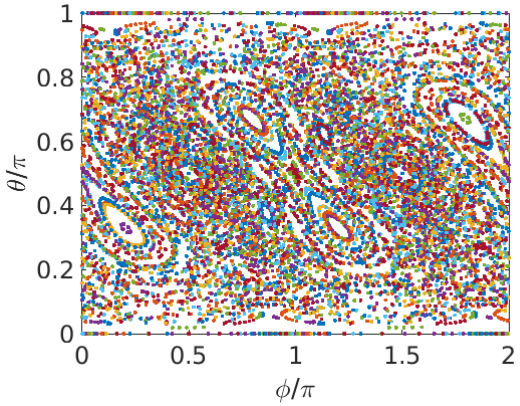

(c) $k = 2.5$

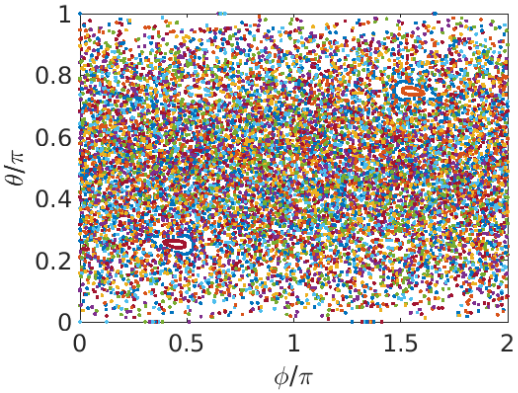

(d) $k = 4.0$

Figure 3.15: Classical trajectories for four values of k

The quantum version follows a similar trend, with the states being spin coherent states $|\theta, \phi\rangle$. The Hamiltonian leads to a unitary evolution such that

$$U_{QKT} = U_{NL}U_{kick}, \qquad U_{NL} = e^{-ikJ_z^2/2j}, \qquad U_{kick} = e^{-ipJ_x}. \tag{3.18}$$

Even though U_{NL} does not commute with U_{kick}, the delta function in the Hamiltonian allows us to write the total unitary as their products. This model is one of the most studied model to study quantum chaos, as it can easily be used to study qubit systems and spin systems. Experimentally, the spin-spin interaction Hamiltonian for the kicked top is given by [27]

$$H_{\mathcal{J}} = 2\pi\mathcal{J}_{23}I_z^1 I_z^2 \tag{3.19}$$

for time τ, such that $\tau = k/2\pi\mathcal{J}_{23}$. For this experiment, We apply π pulses on 2 and 3 to

refocus the spin of the first qubit. The kicks, given by the Hamiltonian

$$H_{rf} = \frac{\pi}{2\Delta}(I_x^1 + I_x^2), \tag{3.20}$$

are applied using rf pulses on both the qubits. The pulse duration is such that $\pi/(2\Delta) = p$. This corresponds to a $\pi/2$ pulse in the x direction. For DBFM, we applied the hard pulse directly, and for TFIE, we used GRAPE to generate the pulses.

3.4.2 Signatures of Chaos

There have been multiple studies to look for quantum signatures of chaos - the quantum quantities, including entanglement and discord, which show chaos in their dynamics [28]. We use the Wigner function to look for signatures of chaos in the model.

We performed experiments on the spin coherent states with the quantum kicked top Hamiltonian to check our theoretical simulations. We selected the chaoticity values $k = 0.5$, where every initial condition is periodic, $k = 2.5$, which has a mixed phase space, and $k = 2\pi + 2.5$, which behaves just like $k = 2.5$ because of the 2π periodicity of the two qubit model. For experiments, we considered different initial states with some in the regular and some in the chaotic region. We selected three points for our experiments, $(\theta, \phi) = (\pi/6, 4\pi/3), (1, 2.5)$ and $(0, 0)$ for their different behaviours under the QKT Hamiltonian.

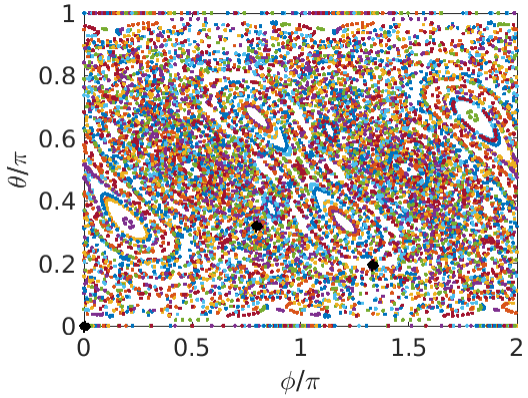

Figure 3.16: The classical kicked top dynamics for $k = 2.5$. The points for our analysis are shown by black solid dots.

We first start with the state $(\theta, \phi) = (\pi/6, 4\pi/3)$, which is in the regular region of the phase space when $k = 2.5, 2\pi + 2.5$. For checking chaos, we only focus on the first row of the Wigner phase space.

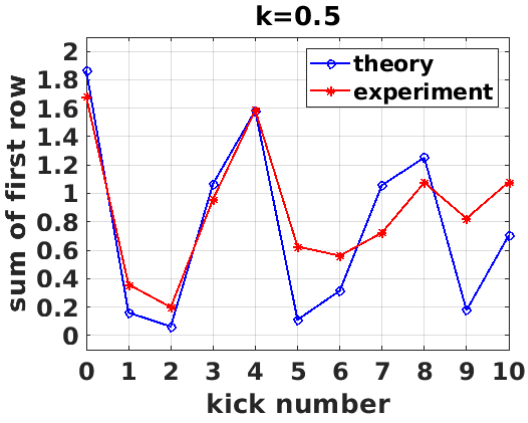

(a) $k = 0.5$

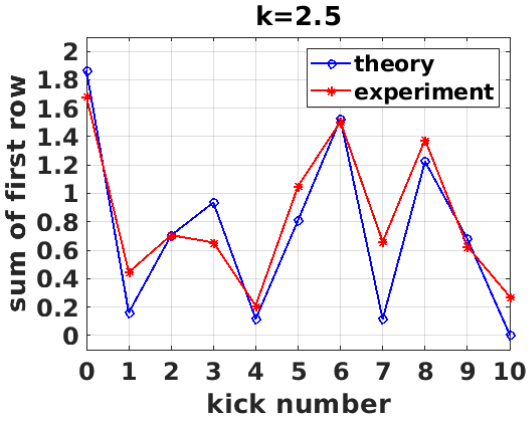

(b) $k = 2.5$

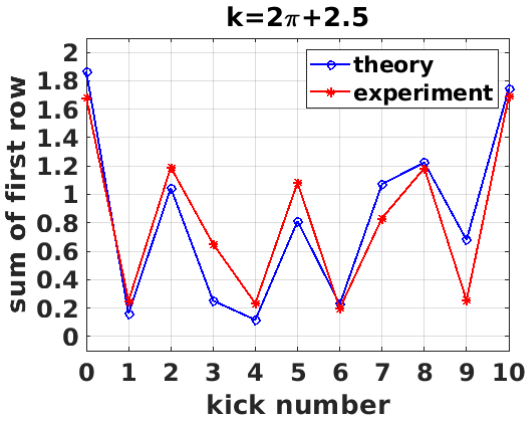

(c) $k = 2\pi + 2.5$

Figure 3.17: Localisation in first row for state $(\theta, \phi) = (\pi/6, 4\pi/3)$

The second state we study is $(\theta, \phi) = (1, 2.5)$, which lies in the chaotic part of the phase space for $k = 2.5, 2\pi + 2.5$.

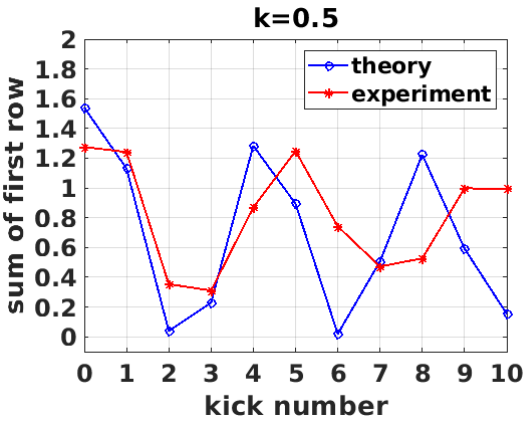

(a) $k = 0.5$

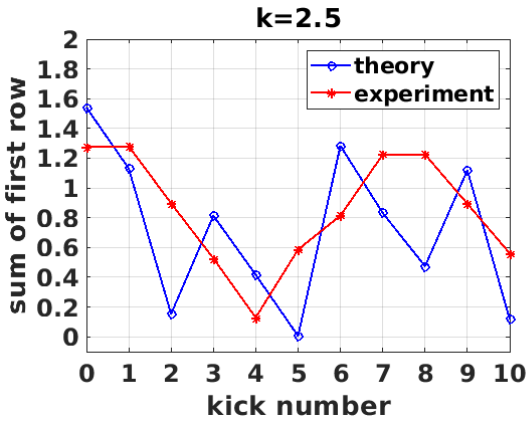

(b) $k = 2.5$

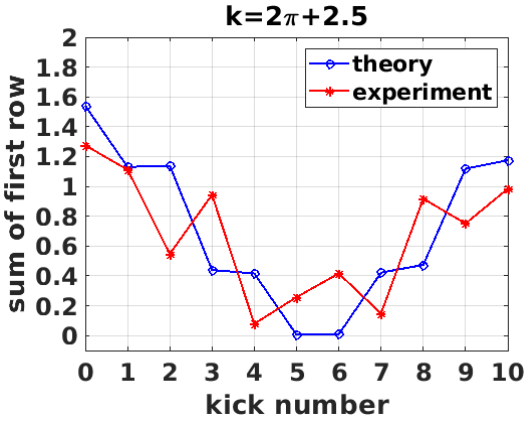

(c) $k = 2\pi + 2.5$

Figure 3.18: Localisation in first row for state $(\theta, \phi) = (1, 2.5)$

Except for the values of the sum being very chaotic by itself, one other way for us to understand the chaoticity in this model is through the very definition of chaoticity, i.e., sensitivity to initial conditions in the model. We see that for the first case, at all values of the chaoticity, the experimental data matches the theoretical prediction very well. However, in the second case, we see that the experimental data is much different from the theory, which we conclude is due to the differences in the initial conditions.

To conclude our studies, we plotted the same data for $(\theta, \phi) = (0, 0)$, which is again supposed to be in the chaotic regime. We see results similar to the previous case, which was also in the chaotic part of the classical phase space.

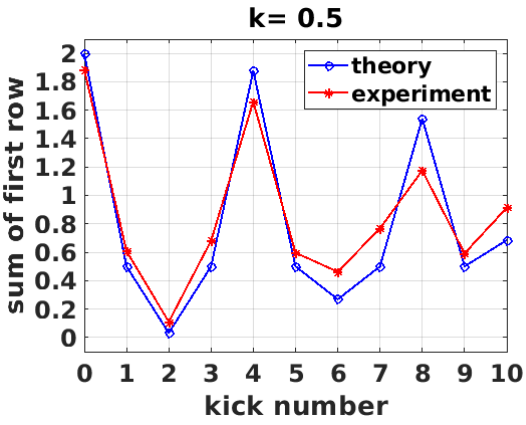

(a) $k = 0.5$

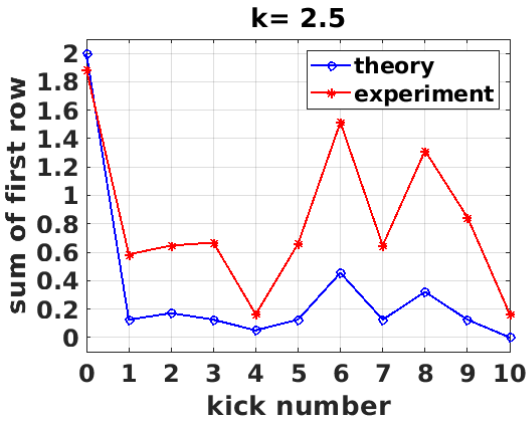

(b) $k = 2.5$

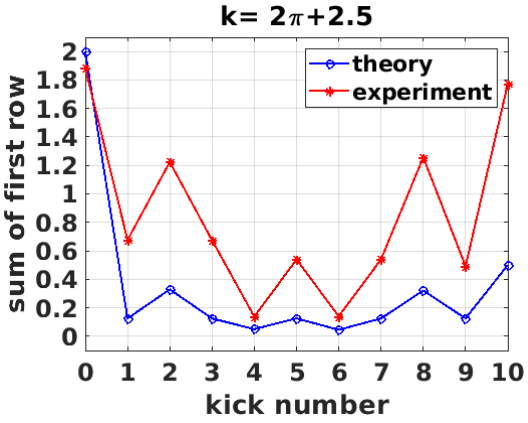

(c) $k = 2\pi + 2.5$

Figure 3.19: Localisation in first row for state $(\theta, \phi) = (0, 0)$

3.4.3 Localized state

Following the result that Gaussian states are localized in the Wigner Phase Space, we created such a state in two qubits. We found that this state also is largely localised in a small number of pixels in the Wigner Phase Space. We now look at the dynamics of the localised state under the quantum kicked top Hamiltonian for different values of the chaoticity parameter.

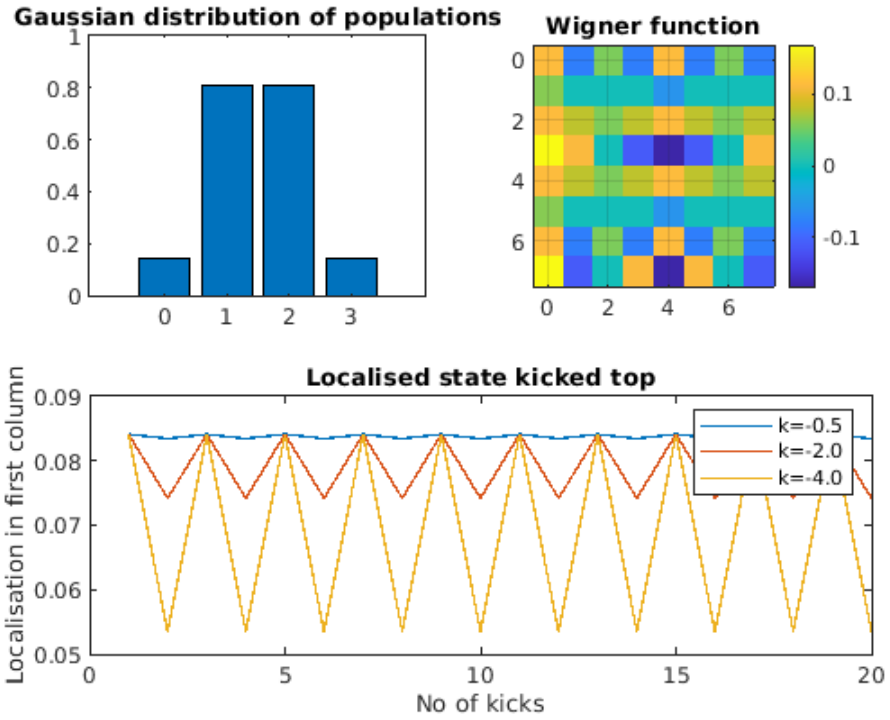

Figure 3.20: Localised state, with evolution under the kicked top Hamiltonian

We found that the various quantities that showed signatures of chaos have periodic dynamics when started with the localised state, even for high chaoticity values. We try to study this state, and the periodic properties in the experiments. We prepared the localised state using the molecule TFIE. The result of the Wigner tomography for the state is given in the figure 3.21.

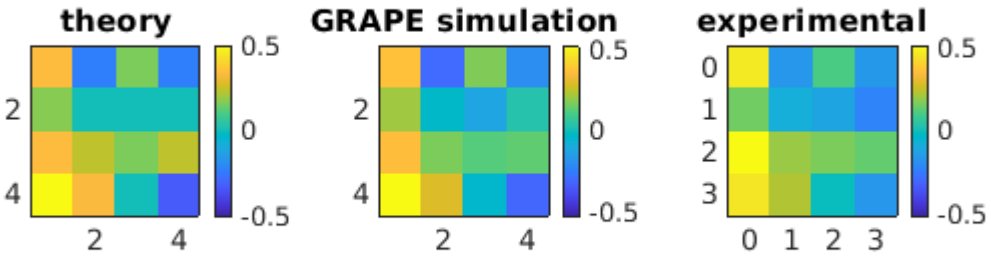

Figure 3.21: Localised state tomography, fidelity 0.9085

Performing the quantum kicked top experiment on the localized state, we find that it matches with the theory with lesser amplitude of oscillations. We observe that the state has a periodicity, as predicted by the simulations, with errors which we attribute to the experimental sources of error, like rf inhomogeneity. This is also shown in the figure 3.22c-3.22d, which shows fidelities of the theory and GRAPE simulations with the experiment. Thus, we claim that this localized state is robust against quantum chaos, at least in some specific Hamiltonians.

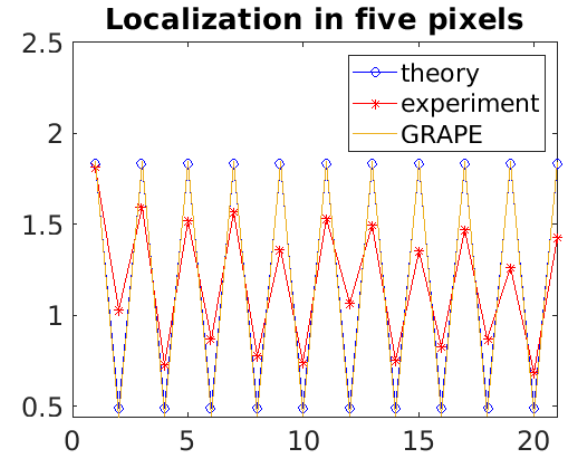

(a) $k = -1$

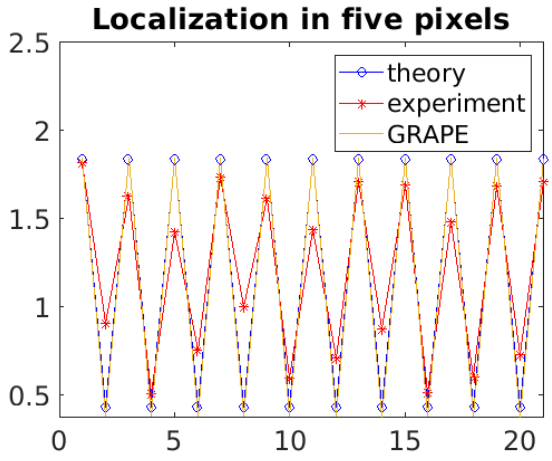

(b) $k = -2$

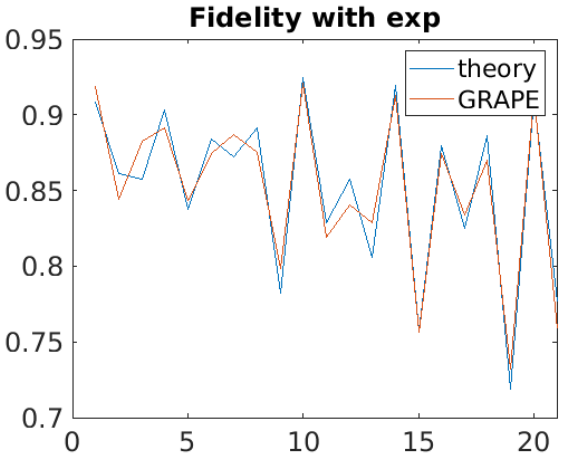

(c) $k = -1$

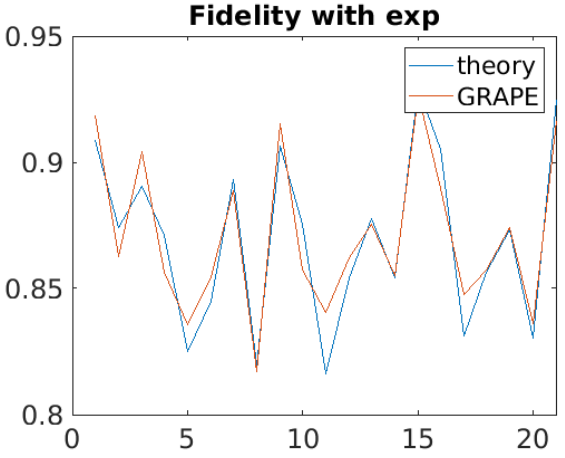

(d) $k = -2$

Figure 3.22: (a)-(b)We take the five pixels the initial state has maximum absolute value in, and plot the sum of them. The x-axis denotes the number of kicks, while the y-axis denotes the sum. (c)-(d) The fidelities of the experimental result with the simulations.

Chapter 4

Conclusion

- In this thesis, we studied the dynamics of different quantum systems and how they correspond from the Liouville space to the Wigner Phase Space.
- Our first objective while working on this topic was to visualize quantum states using the Wigner phase space distribution. We found such a function that has not only a one-to-one correspondence with density matrices, but also is easy to visualize.
- We studied the discrete even-dimensional Wigner phase space and worked out different quantum phenomena using the formalism. We studied the visualizations of these phenomena, which helped us gain a better understanding of them.
- We found a computationally inexpensive least squares regression method to differentiate between amplitude damping, phase damping and depolarization global noise channels in multi-qubit systems. We also found that the same technique can be used to find the contribution of the three types of noise in case they act on the system together. Thus, this method is computationally less expensive than quantum process tomography.
- However, this method cannot be used to find the exact Kraus operators acting on the state. Thus, it gives lesser information than process tomography.
- We performed NMR experiments to measure Wigner functions directly. We used the molecules Dibromofluoromethane (DBFM) and trifluoroiodoethene (TFIE) as our three-qubit quantum registers.

- We found methods to study phase transitions in the Wigner Phase Space, using discontinuities in the entropy of the Wigner Phase Space distribution.
- We also looked at the quantum kicked top experiment using the Wigner Phase Space and found signatures of chaos in the distribution.
- Using localization in the Wigner Phase Space, we found quantum states which are not sensitive to chaos and, thus, can be used effectively in studying quantum chaos.

Outlook

Through our discussions and results on the phase transitions problem, for which we also worked out the adiabatic evolution of a Hamiltonian, we think that the Wigner Phase Space formulation can have applications in non-equilibrium quantum mechanics.

We have taken composite systems here as a single system in this thesis, thus, not going into enough detail about the available correlations in the quantum system. Given the intrinsic connection of the continuous Wigner function with quantum correlations like entanglement [29], we believe that the discrete Wigner distribution has such a connection, which we think can be explored as a follow-up to this study. There might also be non-trivial details in the Wigner function distribution that can be studied to find other measures of quantum correlations, like discord, in the Wigner function.

Another possible direction can be to understand the Wigner function in the classical limit, to study the quantum-classical correspondence principle. We also think this formalism can help us understand quantum computing visually and help develop or optimise algorithms for quantum computing and control applications.

References

1. Goldstein, H., Poole, C. & Safko, J. *Classical Mechanics* (Pearson Education, 2002).
2. Haake, F., Kuś, M. & Scharf, R. Classical and quantum chaos for a kicked top. *Zeitschrift für Physik B Condensed Matter* **65,** 381–395. ISSN: 1431-584X. https://doi.org/10.1007/BF01303727 (1987).
3. Keshavamurthy, S. & Schlagheck, P. *Dynamical Tunneling: Theory and Experiment* ISBN: 9781439816653. https://books.google.co.in/books?id=k4ESQgAACAAJ (Taylor & Francis, 2011).
4. Harriman, J. E. Some properties of the Husimi function. *The Journal of Chemical Physics* **88,** 6399–6408. eprint: https://doi.org/10.1063/1.454477. https://doi.org/10.1063/1.454477 (1988).
5. Drummond, P. D. & Gardiner, C. W. Generalised P-representations in quantum optics. *Journal of Physics A: Mathematical and General* **13,** 2353. https://dx.doi.org/10.1088/0305-4470/13/7/018 (July 1980).
6. Wigner, E. On the Quantum Correction For Thermodynamic Equilibrium. *Phys. Rev.* **40,** 749–759. https://link.aps.org/doi/10.1103/PhysRev.40.749 (5 1932).
7. Moyal, J. E. Quantum mechanics as a statistical theory. *Mathematical Proceedings of the Cambridge Philosophical Society* **45,** 99–124 (1949).
8. Leonhardt, U. Discrete Wigner function and quantum-state tomography. *Phys. Rev. A* **53,** 2998–3013. https://link.aps.org/doi/10.1103/PhysRevA.53.2998 (5 1996).
9. Bertrand, J. & Bertrand, P. A tomographic approach to Wigner's function. *Foundations of Physics* **17,** 397–405. ISSN: 1572-9516. https://doi.org/10.1007/BF00733376 (4 1987).

10. Wootters, W. K. A Wigner-function formulation of finite-state quantum mechanics. *Annals of Physics* **176,** 1–21. ISSN: 0003-4916. https://www.sciencedirect.com/science/article/pii/000349168790176X (1987).

11. Weinbub, J. & Ferry, D. K. Recent advances in Wigner function approaches. *Applied Physics Reviews* **5,** 041104. eprint: https://doi.org/10.1063/1.5046663. https://doi.org/10.1063/1.5046663 (2018).

12. Ferrie, C. Quasi-probability representations of quantum theory with applications to quantum information science. *Reports on Progress in Physics* **74,** 116001. https://dx.doi.org/10.1088/0034-4885/74/11/116001 (2011).

13. Miquel, C., Paz, J. P. & Saraceno, M. Quantum computers in phase space. *Phys. Rev. A* **65,** 062309. arXiv: quant-ph/0204149 [quant-ph] (2002).

14. Cavanagh, J. *Protein NMR Spectroscopy: Principles and Practice. 2nd Ed (9780121644918).* https://books.google.co.in/books?id=a3-xtQEACAAJ (Academic Press, 2007).

15. Hegde, S. S. *Quantum Simulations with Unitary and Nonunitary Controls: NMR implementations* 2017. arXiv: 1701.03443 [quant-ph].

16. Levitt, M. H. *Spin dynamics: basics of nuclear magnetic resonance* (John Wiley & Sons, 2013).

17. Cory, D. G. *et al.* NMR based quantum information processing: Achievements and prospects. *Fortschritte der Physik: Progress of Physics* **48,** 875–907 (2000).

18. Khaneja, N., Reiss, T., Kehlet, C., Schulte-Herbrüggen, T. & Glaser, S. J. Optimal control of coupled spin dynamics: design of NMR pulse sequences by gradient ascent algorithms. *Journal of Magnetic Resonance* **172,** 296–305. ISSN: 1090-7807. https://www.sciencedirect.com/science/article/pii/S1090780704003696 (2005).

19. Miquel, C. *et al.* Interpretation of tomography and spectroscopy as dual forms of quantum computation. *Nature* **418,** 59–62. ISSN: 1476-4687. https://doi.org/10.1038/nature00801 (2002).

20. Batra, P., Krithika, V. R. & Mahesh, T. S. Push-pull optimization of quantum controls. *Phys. Rev. Research* **2,** 013314. https://link.aps.org/doi/10.1103/PhysRevResearch.2.013314 (1 2020).

21. Cory, D. G., Fahmy, A. F. & Havel, T. F. Ensemble quantum computing by NMR-spectroscopy. *Proceedings of the National Academy of Sciences* **94,** 1634–1639. eprint: https://www.pnas.org/doi/pdf/10.1073/pnas.94.5.1634. https://www.pnas.org/doi/abs/10.1073/pnas.94.5.1634 (1997).

22. Golze, D., Icker, M. & Berger, S. Implementation of two-qubit and three-qubit quantum computers using liquid-state nuclear magnetic resonance. *Concepts in Magnetic Resonance Part A* **40A,** 25–37. eprint: https://onlinelibrary.wiley.com/doi/pdf/10.1002/cmr.a.21222 (2012).

23. Nielsen, M. A. & Chuang, I. L. *Quantum Computation and Quantum Information: 10th Anniversary Edition* (Cambridge University Press, 2010).

24. Rao, K. R. K. *et al.* Multipartite quantum correlations reveal frustration in a quantum Ising spin system. *Phys. Rev. A* **88,** 022312. https://link.aps.org/doi/10.1103/PhysRevA.88.022312 (2 Aug. 2013).

25. Zhang, J., Cucchietti, F. M., Laflamme, R. & Suter, D. Defect production in non-equilibrium phase transitions: experimental investigation of the Kibble–Zurek mechanism in a two-qubit quantum simulator. *New Journal of Physics* **19,** 043001. https://dx.doi.org/10.1088/1367-2630/aa6653 (Apr. 2017).

26. Damski, B. & Zurek, W. H. Adiabatic-impulse approximation for avoided level crossings: From phase-transition dynamics to Landau-Zener evolutions and back again. *Phys. Rev. A* **73,** 063405. https://link.aps.org/doi/10.1103/PhysRevA.73.063405 (6 June 2006).

27. Krithika, V. R., Anjusha, V. S., Bhosale, U. T. & Mahesh, T. S. NMR studies of quantum chaos in a two-qubit kicked top. *Phys. Rev. E* **99,** 032219. https://link.aps.org/doi/10.1103/PhysRevE.99.032219 (3 2019).

28. Madhok, V., Gupta, V., Trottier, D.-A. & Ghose, S. Signatures of chaos in the dynamics of quantum discord. *Phys. Rev. E* **91,** 032906. https://link.aps.org/doi/10.1103/PhysRevE.91.032906 (3 Mar. 2015).

29. Arkhipov, I. I., Barasiński, A. & Svozilık, J. Negativity volume of the generalized Wigner function as an entanglement witness for hybrid bipartite states. *Scientific reports* **8,** 16955 (2018).